Extracavity effect in cyclodextrin/surfactant complexation

Vargas, Carolyn; Schönbeck, Jens Christian Sidney; Heimann, Ina; Keller, Sandro

Published in:
Langmuir

DOI:
10.1021/acs.langmuir.8b00682

Publication date:
2018

Document Version
Peer reviewed version

Citation for published version (APA):
Vargas, C., Schönbeck, J. C. S., Heimann, I., & Keller, S. (2018). Extracavity effect in cyclodextrin/surfactant complexation. *Langmuir*, *34*(20), 5781–5787. https://doi.org/10.1021/acs.langmuir.8b00682

Extra-cavity effect in cyclodextrin/surfactant complexation

Carolyn Vargas,[†] Christian Schönbeck,[‡] Ina Heimann,[†] and Sandro Keller[†*]

†Molecular Biophysics, Technische Universität Kaiserslautern (TUK), Erwin-Schrödinger-Str. 13, 67663 Kaiserslautern, Germany

‡Department of Science and Environment, Roskilde University, Universitetsvej 1, 4000 Roskilde, Denmark

ABSTRACT: Cyclodextrin (CD) complexation is a convenient method to sequester surfactants in a controllable way, for example, during membrane-protein reconstitution. Interestingly, the equilibrium stability of CD/surfactant inclusion complexes increases with the length of the nonpolar surfactant chain even beyond the point where all hydrophobic contacts within the canonical CD cavity are saturated. To rationalize this observation, we have dissected the inclusion complexation equilibria of a structurally well-defined CD, that is, heptakis(2,6-di-*O*-methyl)-β-CD (DIMEB), and a homologous series of surfactants, namely, *n*-alkyl-*N*,*N*-dimethyl-3-ammonio-1-propanesulfonates (SB3-*x*) with chain lengths ranging from $x = 8$ to 14. A combination of thermodynamic parameters obtained by isothermal titration calorimetry (ITC) and structural insights derived from nuclear magnetic resonance (NMR) spectroscopy and molecular dynamics (MD) simulations revealed that, upon inclusion, long-chain surfactants with $x \geq 10$ extend beyond the canonical CD cavity. This enables the formation of hydrophobic contacts between long surfactant chains and the extra-cavity parts of DIMEB, which make additional favorable contributions to the stability of the inclusion complex. These results explain the finding that the stability of CD/surfactant inclusion complexes monotonously increases with surfactant chain length even for long chains that completely fill the canonical CD cavity.

INTRODUCTION

Cyclodextrin (CD) complexation of surfactants plays an important role in many fields of basic and applied research. For example, CD complexation offers an efficient and controllable means of removing surfactants from membrane-protein reconstitution mixtures. In contrast with other approaches relying on hydrophobic surface adsorption rather than supramolecular inclusion, surfactant complexation by CDs displays defined stoichiometries and tunable affinities.[1] Most CDs frequently used in membrane-protein research are highly water-soluble derivatives of β-CD such as randomly methylated β-CD (MβCD),[2] 2-hydroxypropyl-β-CD (HPβCD),[3] and heptakis(2,6-di-*O*-methyl)-β-CD (DIMEB).[4–6] These CDs are composed of seven α(1–4)-linked glucopyranoside units, which together assume the shape of a truncated cone. Modified primary O6 and secondary O2 and O3 hydroxyl groups form the narrower and wider rims, respectively, of this truncated cone. The hydrophobic CD cavity is lined by a glycosidic oxygen bridge and the hydrogens of carbon atoms 3 and 5 of each glucopyranose unit (Chart 1). This cavity can bind a very broad range of chemically diverse small hydrophobic molecules, including sterols such as cholesterol[7] and surfactant alkyl chains,[1] both of which play important roles in membrane-protein research.

We have recently demonstrated the calorimetric quantification and modeling of linked equilibria in CD/surfactant/lipid(/protein) mixtures.[8,9] The predictive power and, thus, the practical utility of such quantitative models critically depend on the accurate quantification of the equilibrium stability of the CD/surfactant inclusion complex in question.[8,9] Previous studies[10–22] have found that complex stability monotonously increases with surfactant chain length, but it has remained unclear why this is so even for surfactants whose nonpolar chains are so long that they reach across the CD ring. In these cases, all potential hydrophobic contacts within the canonical CD cavity are established, so that further elongation of the surfactant chain can make no additional contributions to such interactions.

To address this question, we focused on the interactions between a modified β-CD, namely, DIMEB, and a homologous surfactant series comprising *n*-alkyl-*N*,*N*-dimethyl-3-ammonio-1-propanesulfonates (SB3-*x*). Here, *x* denotes the number of carbon atoms in the alkyl chain, that is, $x = 8$, 10, 12, or 14 (Chart 1). This range of chain lengths allowed us to systematically analyze variations in the inclusion depth of the surfactant chain inside the DIMEB cavity and the consequences of extending the chain such that it protrudes beyond the cavity. Unlike previous reports employing randomly substituted CDs, we chose DIMEB because it is structurally defined with a degree of substitution (DS) of ~14, thus eliminating issues due to variabilities in the degree and pattern of CD substitution.[23] Moreover, the high aqueous solubility of DIMEB allows high-quality data with excellent signal/noise (S/N) ratios to be obtained from both calorimetric and spectroscopic experiments over broad temperature and concentration ranges.

We compared thermodynamic quantities derived from high-sensitivity isothermal titration calorimetry (ITC) with structural insights obtained from nuclear magnetic resonance (NMR) spectroscopy and molecular dynamics (MD) simulations to examine the interactions between DIMEB and SB3-*x* of different alkyl chain lengths. Since the affinity of DIMEB for SB3-*x* was found to increase as the chain was extended beyond the canonical CD cavity, we closely investigated the additional interactions present in long-chain but absent from short-chain SB3-*x* with the aid of NMR rotating-frame Overhauser spectroscopy (ROESY) experiments and MD simulations to identify the contributions that lead to more stable complexes. Experiments and simulations consistently revealed an increase in the burial of nonpolar surface area upon complexation with increasing surfactant chain length even though longer chains did not result in the inclusion of more hydrocarbon chain inside the cavity. Rather, the stronger binding of long-chain surfactants was found to be owed to extra-cavity hydrophobic interactions with the rim of the CD ring.

EXPERIMENTAL

2.1 Materials. DIMEB (purity ~95%, DS ~14) was purchased from Cyclolab (Budapest, Hungary). *n*-octyl-*N*,*N*-dimethyl-3-ammonio-1-propanesulfonate (SB3-8) was purchased from Merck (Darmstadt, Germany); all other surfactants were from Anatrace (Maumee, USA). $NaH_2PO_4 \cdot 2H_2O$, Na_2HPO_4, and D_2O were obtained from Sigma–Aldrich (Steinheim, Germany), and NaCl was from VWR (Darmstadt, Germany). All chemicals were of the highest purity available.

2.2 Isothermal titration calorimetry. Calorimetric measurements were performed on a MicroCal Auto-iTC$_{200}$ (Malvern Instruments, Malvern, UK) with an injection volume of 2 µL, a time spacing of 360 s, a filter period of 5 s, a stirring speed of 750 rpm, and a reference power of 21 µJ s^{-1}. All solutions were prepared in buffer containing 50 mM NaH_2PO_4/Na_2HPO_4, 50 mM NaCl, pH 7.4. The syringe was loaded with 5, 10, or 20 mM DIMEB, and the reference cell was filled with buffer. 500-µL aliquots of 0.5, 1, or 2 mM SB3-*x* solutions (and buffer for control titrations) were loaded in triplicates into 96-well plates for automated serial filling of the sample cell. Automated experiments were performed across a temperature range of 10–48°C. To analyze raw thermograms, baseline assignment by singular-value decomposition and peak integration were performed using NITPIC.[24] Isotherms were analyzed by nonlinear least-squares fitting in SEDPHAT[25] using a one-site binding model. Relatively shallow isotherms were obtained for DIMEB/SB3-8 and DIMEB/SB3-10; hence, the correction factor for the cell (i.e., SB3-*x*) concentration was fixed at $n = 1$ to avoid overparameterization. For the other surfactants studied, n was allowed to float but was always found to be close to 1.0. For each surfactant, three different DIMEB/SB3-*x* concentration pairs at six different temperatures were globally analyzed, and 95% confidence intervals were determined by error-surface projection.[26]

2.3 Nuclear magnetic resonance spectroscopy. All NMR experiments were performed on a Bruker Avance spectrometer (Rheinstetten, Germany) operating at 400.33 MHz proton frequency, equipped with a 5-mm broadband inverse probe. All data were acquired in D_2O at 25°C using standard pulse sequences. Proton chemical shifts of DIMEB[27] and each SB3-*x*[28] were assigned and referenced to the residual HOD signal at 4.7 ppm. 2D NMR ROESY spectra of solutions containing 10 mM DIMEB and 10 mM SB3-*x* were recorded using a mixing time of 300 ms, a relaxation delay of 3 s, 32 scans, and a total of 1024 data points in $F2$ and 256 data points in $F1$ over a spectral width of 2000 Hz.

2.4 Molecular dynamics simulations. MD simulations were carried out in NAMD[29] using the CHARMM carbohydrate force field[30,31] for the unsubstituted CD structure. Parameters for the CD methyl groups and the SB3-*x* guests were generated with the CGenFF program[32,33] (version 1.0.0) and the CHARMM General Force Field[34] (version 3.0.1). Initial structures of the complexes were generated by placing the SB3-*x* guests inside the CD with the headgroup protruding from the secondary rim. Simulations were run with periodic boundary conditions in cubic boxes filled with TIP3P water, ranging in size from 40 × 40 × 40 Å^3 for the shortest surfactant to 46 × 46 × 46 Å^3 for the longest. All free species were simulated for 20 ns and the complexes for 30 ns, all with 2-fs time steps. The first 2 ns of equilibration were not included in subsequent analyses. The accessible surface area (ASA) was measured with a probe radius of 1.4 Å. All simulations were prepared, visualized, and analyzed in VMD.[35]

RESULTS AND DISCUSSION

3.1 DIMEB binds longer-chain SB3-*x* more tightly. We used high-sensitivity ITC to determine the molar changes in standard Gibbs free energy, enthalpy, entropy, and isobaric heat capacity upon DIMEB binding of each SB3-*x*. ITC datasets obtained at three different DIMEB/SB3-*x* concentration pairs over a temperature range of 10–48°C were globally analyzed[25] by assuming a 1:1 binding model (Figure 1). The best-fit values and associated 95% confidence intervals thus derived are summarized in Table 1. Data points that were affected by the presence of surfactant micelles in a few experiments were excluded from the fitting procedure. Thus, good global fits were obtained for all data, indicating that DIMEB formed 1:1 complexes with all SB3-*x* tested. It is well known that, in addition to 1:1 associations, some CDs form higher-order complexes with acyl chains of phospholipids[36,37] or long-chain surfactants.[38] However, this phenomenon is not observed for all CDs, as demonstrated in our previous study for HPβCD[9] or here for DIMEB/SB3-*x* complexes. In the latter case, the molar change in Gibbs free energy upon binding, $\Delta G°$, increased in magnitude from –16.4 to –27.6 kJ mol^{-1} as the chain length of SB3-*x* increased from 8 to 14. Specifically, the binding affinity steadily increased with the number of methylene groups in the hydrophobic tail of the surfactant. The accompanying molar changes in enthalpy, $\Delta H°$, and in the entropic term, $-T\Delta S°$, ranged from 6.4 to 3.0 kJ mol^{-1} and from –22.8 to –30.6 kJ mol^{-1}, respectively, thus reflecting a less unfavorable enthalpic and, to a greater degree, a more favorable entropic contribution for longer chains. $\Delta G°$, $\Delta H°$, and $-T\Delta S°$ values are plotted as functions of chain length, *x*, in Figure 2. The formation of inclusion complexes was accompanied by a large reduction in isobaric heat capacity, ΔC_p, which increased in magnitude from –375 to –664 J mol^{-1} K^{-1} when *x* increased from 8 to 14. Negative heat capacity changes are commonly attributed to the dehydration of nonpolar surface area, which in the case of CD inclusion affects both the guest molecule and the CD cavity.[39] Area-based models are frequently used to correlate ΔC_p to the ASA of the guest molecule.[40,41] Thus, we explored this relationship by MD simulations guided by NMR data to examine the contributions of each methylene group to ΔC_p and subsequently relate them to the amount of hydrophobic surface area buried upon binding.

3.2 Longer SB3-*x* chains extend beyond the CD cavity. MD simulations of all free—that is, unbound—SB3-*x* species revealed bent conformations of the alkyl chain, with an angle of ~90° about the nitrogen atom (Figure 3), presumably to minimize steric clash between the methyl groups attached to the nitrogen and the methylene groups on the chain. This conformation was similarly observed in MD simulations when the surfactant was bound to DIMEB. No dissociation of the complexes was observed among the complexed species; however, a slight tendency to crawl out of the cavity was detected for the shortest-chain surfactant, SB3-8, suggesting relatively weak inclusion in the cavity, consistent with our ITC results. Notably, for long chain-surfactants, a considerable part of the chain is not included within the canonical CD cavity, but the SB3-*x* molecule as a whole remains bound to DIMEB. The predominant inclusion mode of DIMEB/SB3-*x* complexes, as used for MD simulations, was confirmed by NMR ROESY experiments. The latter revealed correlations between the methylene protons at C2 of SB3-*x* and the H3 protons of DIMEB, which are located in interior of the cavity near the wider secondary rim. Moreover, correlations between the terminal methyl groups of SB3-*x* and the methyl groups on O6 of DIMEB (O6-CH_3) suggested that the headgroup of the surfactant protruded from the CD secondary rim (Figure 4). In the simulations, the SB3-8 hydrocarbon chain hardly protruded from the primary rim (Video S1 in SI), in contrast with all longer-chain SB3-*x* species (i.e., for $x = 10$, 12, or 14). These longer chains protruded from the primary rim and interacted with the methyl groups on O6 of DIMEB (Video S2 in SI). Methyl groups on O2 of DIMEB (O2-CH_3) pointed away from the cavity, and no interactions were seen with the surfactant chain. All bound SB3-*x* chains were found to be uncoiled in the interior of the CD cavity, and no water molecules were observed within the cavity together with the surfactant.

3.3 Extra-cavity effects enhance binding of longer SB3-*x*. Following the characterization of free and complexed species by MD simulations, we calculated their polar and nonpolar surface areas that are accessible to water, ASA_{pol} and ASA_{nonpol}, respectively. As expected, ASA_{pol} of free SB3-*x* was almost independent of chain length, with only 1–2 Å^2 variations. By contrast, ASA_{nonpol} increased linearly with chain length with an increment of 28.7 Å^2 per methylene group. This is slightly lower than the value reported for alkanes (31.5 Å^2).[42] Upon complexation, the change in ASA_{nonpol}, ΔASA_{nonpol}, which reflects the hydrophobic surface area buried upon inclusion of surfactant into DIMEB, decreased linearly with an increment of –21.5 Å^2 per methylene group (Figure 5a). Using an averaged experimental literature value for the contribution to ΔC_p of 1.8 J mol^{-1} K^{-1} for each Å^2 of buried surface,[43] this translates into a contribution to ΔC_p of approximately –40 J mol^{-1} K^{-1} per methylene group. This calculated value correlates reasonably well with the experimentally determined contribution to ΔC_p of –48.1 J mol^{-1} K^{-1} per methylene group (Figure 5b), given that literature values for the contribution of hydrophobic burial to ΔC_p range from 1.2 to 2.2 J mol^{-1} K^{-1} Å^{-2}.[41,44] Plotting our experimental ΔC_p values as a function of ΔASA_{nonpol} obtained from simulations yielded 2.2 J mol^{-1} K^{-1} Å^{-2} (Figure 5c), hence corroborating the quantitative correlation between ΔASA_{nonpol} and ΔC_p.

We further analyzed the contributions from individual atoms making up the surfaces of DIMEB and SB3-*x* to determine which parts of the molecules are buried upon complexation. The MD simulations showed that most of the buried nonpolar surface belonged to SB3-*x*. However, the increment in ΔASA_{nonpol} with increasing chain length was brought about by the burial of equally large areas of DIMEB and SB3-*x*, as reflected in similar slopes (Figure 6a). All alkyl chains tested completely filled up the canonical CD cavity, that is, the inner part of the heptaglucopyranose ring. Specifically, protons H3 and H5 inside the DIMEB cavity were found to be extensively dehydrated irrespective of SB3-*x* chain length (Figure 6b). Accordingly, the enhanced binding affinities of longer-chain surfactants were exclusively due to additional hydrophobic contacts with 6-CH_2 on the narrow, primary rim of DIMEB. For this moiety, the extent of dehydration clearly depended on alkyl chain length. From SB3-8 to SB3-12, a substantial increase in the burial of 6-CH_2 was observed, while there was hardly any increase from SB3-12 to SB3-14 (Figure 6b). Interestingly, this trend correlated well with $\Delta G°$ for complexation, suggesting that establishing extra-cavity hydrophobic contacts contributed substantially to the observed increase in binding affinity with SB3-*x* chain length (Figure 2). Conversely, the ΔASA_{nonpol} values of the alkyl chains increased with chain length as, in addition to the inclusion of the central parts of SB3-*x* within the canonical CD cavity, 9-CH_2 to 14-CH_3 became dehydrated upon interaction with 6-CH_2 of DIMEB (Figure 6c) in the case of longer-chain surfactants.

So far, we have shown that longer-chain SB3-12 and SB3-14 led to increased burial of O6-CH_3, which was not easily accessible to short-chain SB3-8 and SB3-10. By contrast, the hydrophobic contacts with O2-CH_3 on the secondary side of DIMEB were almost invariant with chain length, as the SB3-*x* chains projected exclusively from the primary side, as confirmed by our ROESY data. To dissect this in greater detail, we evaluated the parts of SB3-*x* that were included in the CD cavity with the latter being defined as a sphere with a radius of 3 Å centered on the geometric center of the glycosidic oxygens and the H5 protons of DIMEB (Figure 7a). Histograms displaying the percentage of the total time spent inside the cavity by each of the carbon atoms of SB3-*x* (Figure 7b) were similar for all complexes. These data thus demonstrated that the cavity primarily accommodated the central parts of SB3-*x*, whereas the longer hydrocarbon chains extended from the primary rim of DIMEB. This was supported by the ROESY data that showed an increase in correlation peak intensity for the methyl groups of SB3-*x* with O6-CH_3 (Figure 4). In summary, extending the surfactant length beyond SB3-8 mainly resulted in more of the hydrocarbon tail protruding from the primary CD rim to engage in additional hydrophobic contacts with O6-CH_3 groups and H6 of DIMEB, thus leading to the formation of more stable DIMEB/SB3-*x* complexes.

CONCLUSIONS

We investigated the equilibrium interactions between a structurally well-defined DIMEB and a homologous series of surfactants of increasing alkyl chain length. A combination of thermodynamic information gleaned from ITC as well as structural data from NMR experiments and MD simulations consistently demonstrated that chain extensions that reach beyond the canonical CD cavity form additional hydrophobic contacts with the extra-cavity parts of DIMEB (i.e., O6-CH_3), thereby contributing to the increased stability of inclusion complexes involving long-chain surfactants.

AUTHOR INFORMATION

Corresponding Author

*Email: mail@sandrokeller.com

ORCID

Carolyn Vargas: 0000-0001-7871-5004
Christian Schönbeck: 0000-0003-4299-3744
Sandro Keller: 0000-0001-5469-8772

Notes

The authors declare no competing financial interests.

Author Contributions

The manuscript was written through contributions of all authors. All authors have given approval to the final version of the manuscript.

ACKNOWLEDGMENTS

We thank Dr. Harald Kelm (Technische Universität Kaiserslautern) for assistance with NMR. Malvern Instruments and, in particular, Dr. Natalia Markova, are gratefully acknowledged for access to their Auto-iTC$_{200}$. This work was partly funded by the Deutsche Forschungsgemeinschaft (DFG) through grant no. KE 1478/4-1. C. S. is supported by a grant (DFF–5054-00173) from the Danish Council for Independent Research.

REFERENCES

(1) DeGrip, W. J.; Vanoostrum, J.; Bovee-Geurts, P. H. M. Selective detergent-extraction from mixed detergent/lipid/protein micelles, using cyclodextrin inclusion compounds: a novel generic approach for the preparation of proteoliposomes. *Biochem. J.* **1998**, *330*, 667–674.

(2) Signorell, G. A.; Kaufmann, T. C.; Kukulski, W.; Engel, A.; Rémigy, H. W. Controlled 2D crystallization of membrane proteins using methyl-β-cyclodextrin. *J. Struc. Biol.* **2007**, *157*, 321–328.

(3) Stokes, D. L.; Ubarretxena-Belandia, I.; Gonen, T.; Engel, A. High-throughput methods for electron crystallography. *Methods Mol. Biol.* **2013**, *955*, 273–296.

(4) Pandit, A.; Shirzad-Wasei, N.; Wlodarczyk, L. M.; van Roon, H.; Boekema, E. J.; Dekker, J. P.; de Grip, W. J. Assembly of the major light-harvesting complex II in lipid nanodiscs. *Biophys. J.* **2011**, *101*, 2507–2515.

(5) Ratnala, V. R. P.; Swarts, H. G. P.; VanOostrum, J.; Leurs, R.; DeGroot, H. J. M.; Bakker, R. A.; DeGrip, W. J. Large-scale overproduction, functional purification and ligand affinities of the His-tagged human histamine H1 receptor. *Eur. J. Biochem.* **2004**, *271*, 2636–2646.

(6) Schenck, S.; Wojcik, S. M.; Brose, N.; Takamori, S. A chloride conductance in VGLUT1 underlies maximal glutamate loading into synaptic vesicles. *Nat. Neurosci.* **2009**, *12*, 156–162.

(7) Mahammad, S.; Parmryd, I. Cholesterol depletion using methyl-β-cyclodextrin. *Methods Mol. Biol.* **2015**, *1232*, 91–102.

(8) Textor, M.; Vargas, C.; Keller, S. Calorimetric Quantification of linked equilibria in cyclodextrin/lipid/detergent mixtures for membrane-protein reconstitution. *Methods* **2015**, *76*, 183–193.

(9) Textor, M; Keller, S. Calorimetric quantification of cyclodextrin-mediated detergent extraction for membrane-protein reconstitution. *Methods Enzymol.* **2016**, *567*, 129–156.

(10) Satake, S.; Yoshida, S.; Hayakawa. K.; Maeda, T.; Kusumoto, Y. Conductometric determination of the association constants of β-cyclodextrin with amphiphilic ions. *Bull. Chem. Soc. Jpn.* **1986**, *59*, 3991–3993.

(11) Palepu, R.; Richardson, J. E.; Reinsborough, V. C. Binding constants of β-cyclodextrin/surfactant inclusion by conductivity measurements. *Langmuir* **1989**, *5*, 218–221.

(12) Bastos, M; Briggner, L. E.; Shehatta, I.; Wadsö, I. The binding of alkane-α-ω-diols to α-cyclodextrin. A microcalorimetric study. *J. Chem. Thermodynamics* **1990**, *22*, 1181–1190.

(13) Wilson, L. D.; Siddall, S. R.; Verrall, R. E. A spectral displacement study of the binding constants of cyclodextrin–hydrocarbon and –fluorocarbon surfactant inclusion complexes. *Can. J. Chem.* **1997**, *75*, 927–933.

(14) De Lisi, R.; Milioto, S.; Muratore, N. Thermodynamic properties of sodium *n*-Alkanecarboxylates in water and in water + cyclodextrins mixtures. *Langmuir* **1998**, *14*, 6045–6053.

(15) Wilson, L. D.; Verrall, R. E. Volumetric study of modified β-cyclodextrin/hydrocarbon and /fluorocarbon surfactant inclusion complexes in aqueous solutions. *J. Phys. Chem. B* **1998**, *102*, 480–488.

(16) Eli, W.; Chen, W.; Xue, Q. The association of anionic surfactants with β-cyclodextrin. An isothermal titration calorimeter study. *J. Chem. Thermodynamics* **1999**, *31*, 1283–1296.

(17) Stödeman, M.; Gòmez-Orellana, I.; Hallén, D. Thermodynamics of binding of α-cyclodextrin to straight-chain alkyl derivatives in aqueous solution. *J. Incl. Phenom. Macrocycl. Chem.* **2003**, *46*, 125–132.

(18) Vega-Rodriguez, A.; Piñeiro, Á.; Perez-Casas, S. Thermodynamics of the interaction between hydroxypropyl-α-cyclodextrin and alkanols in aqueous solutions. *Thermochim. Acta* **2003**, *405*, 109–115.

(19) Castronuovo, G.; Niccoli, M. Complexation of natural and methylated β-cyclodextrins with long-chain carboxylic acids in aqueous solutions. Calorimetric studies at 298 K. *J. Incl. Phenom. Macrocycl. Chem.* **2005**, *53*, 69–76.

(20) Valente, A. J. M.; Dinis, C. J. S.; Pereira, R. F. P.; Ribeiro, A. C. F.; Lobo, V. M. M. Interactions between β-cyclodextrin and some sodium alkyl sulfates and sulfonates as seen by electrical conductivity measurements. *Portugaliae Electrochimica Acta* **2006**, *24*, 129–136.

(21) Castronuovo, G.; Niccoli, M. The cavity elongation effect. Calorimetric studies of the complexes of long-chain carboxylic acids with methyl-α-cyclodextrin in aqueous solutions. *J. Incl. Phenom. Macrocycl. Chem.* **2007**, *58*, 289–294.

(22) Benkő, M.; Tabajdi, R.; Király, Z. Thermodynamics of formation of β-cyclodextrin inclusion complexes with four series of surfactant homologs. *J. Therm. Anal. Calorim.* **2013**, *112*, 969–976.

(23) Schönbeck, C.; Westh, P.; Madsen, J. C.; Larsen, K. L.; Städe, L. W.; Holm, R. Methylated β-Cyclodextrins: Influence of degree and pattern of substitution on the thermodynamics of complexation with tauro- and glyco-conjugated bile salts. *Langmuir* **2011**, *27*, 5832–5841.

(24) Keller, S.; Vargas, C.; Zhao, H.; Piszczek, G.; Brautigam, C. A.; Schuck, P. High-precision isothermal titration calorimetry with automated peak-shape analysis. *Anal. Chem.* **2012**, *84*, 5066–5073.

(25) Houtman, J. C.; Brown, P. H.; Bowden, B.; Yamaguchi, H.; Appella, E.; Samelson, L. E.; Schuck, P. Studying multisite binary and ternary protein interactions by global analysis of isothermal titration calorimetry data in SEDPHAT: application to adaptor protein complexes in cell signaling. *Protein Sci.* **2007**, *16*, 30−42.

(26) Kemmer, G.; Keller, S. Nonlinear least-squares data fitting in Excel spreadsheets. *Nat. Prot.* **2010**, *5*, 267–281.

(27) Correia, I.; Bezzenine, N.; Ronzani, N.; Platzer, N.; Beloeil, J. C.; Doan, B. T. Study of inclusion complexes of acridine with β- and (2,6-di-*O*-methyl)-β-cyclodextrin by use of solubility diagrams and NMR Spectroscopy. *J. Phys. Org. Chem.* **2002**, *15*, 647–659.

(28) Mascioni, A.; Moy, F. J.; McNeil, L. K.; Murphy, E.; Bentley, B. E.; Camarda, R.; Dilts, D. A.; Fink, P. S.; Gusarova, V.; Hoiseth, S. K.; et al. NMR dynamics and antibody recognition of the meningococcal lipidated outer membrane protein LP2086 in micellar solution. *Biochim. Biophys. Acta* **2007**, *1798*, 87–93.

(29) Phillips, J. C.; Braun, R.; Wang, W.; Gumbart, J.; Tajkhorshid, E.; Villa, E.; Chipot, C.; Skee,l R. D.; Kalé, L.; Schulten, K. Scalable molecular dynamics with NAMD. *J. Comput. Chem.* **2005**, *26*, 1781–1802.

(30) Guvench, O.; Green, S. N.; Kamath, G.; Brady, J. W.; Venable, R. M.; Pastor, R. W.; Mackerell, A. D. Jr. Additive empirical force field for hexopyranose monosaccharides. *J. Comput. Chem.* **2008**, *29*, 2543–2564.

(31) Guvench, O.; Hatcher, E.; Venable, R. M.; Pastor, R. W.; MacKerell, A. D. CHARMM additive all-atom force field for glycosidic linkages between hexopyranoses. *J. Chem. Theory Comput.* **2009**, *5*, 2353–2370.

(32) Vanommeslaeghe, K.; MacKerell, A. D. Automation of the CHARMM general force field (CGenFF) I: bond perception and atom typing. *J. Chem. Inf. Model.* **2012**, *52*, 3144–3154.

(33) Vanommeslaeghe, K.; Raman, E. P.; MacKerell, A. D. Automation of the CHARMM general force field (CGenFF) II: assignment of bonded parameters and partial atomic charges. *J. Chem. Inf. Model.* **2012**, *52*, 3155–3168.

(34) Vanommeslaeghe, K.; Hatcher, E.; Acharya, C.; Kundu, S.; Zhong, S.; Shim, J.; Darian, E.; Guvench, O.; Lopes, P.; Vorobyov, I.; Mackerell, A. D. Jr. CHARMM general force field: a force field for drug-like molecules compatible with the CHARMM all-atom additive biological force fields. *J. Comput. Chem.* **2010**, *31*, 671–690.

(35) Humphrey, W.; Dalke, A.; Schulten, K. VMD: Visual molecular dynamics. *J. Mol. Graph.* **1996**, *14*, 33–38.

(36) Anderson, T. G; Tan, A.; Ganz, P.; Seelig, J. Calorimetric measurement of phospholipid interaction with methyl-β-cyclodextrin. *Biochemistry* **2004**, *43*, 2251–2261.

(37) Markones, M.; Drechsler, C.; Kaiser, M.; Kalie, L.; Heerklotz, H.; Fiedler, S. Engineering asymmetric lipid vesicles: accurate and convenient control of the outer leaflet lipid composition. *Langmuir* **2018**, *34*, 1999–2005.

(38) Funasaki, N.; Ishikawa, S.; Neya, S. 1:1 and 1:2 Complexes between long-chain surfactant and α-cyclodextrin studied by NMR. *J. Phys. Chem. B* **2004**, *108*, 9593–9598.

(39) Ross, P.D.; Rekharsky, M. V. Thermodynamics of hydrogen bond and hydrophobic interactions in cyclodextrin complexes. *Biophys. J.* **1996**, *71*, 2144–2154.

(40) Spolar, R. S.; Livingstone, J. R.; Record, M. T. Jr. Use of liquid hydrocarbon and amide transfer data to estimate contributions to thermodynamic functions of protein folding from the removal of nonpolar and polar surface from water. *Biochemistry* **1992**, *31*, 3947–3955.

(41) Schönbeck, C.; Holm, R.; Westh, P.; Peters, G. H. Extending the hydrophobic cavity of β-cyclodextrin results in more negative heat capacity changes but reduced binding affinities. *J. Incl. Phenom. Macrocycl. Chem.* **2014**, *78*, 351–361.

(42) Gallicchio, E.; Kubo, M. M.; Levy, R. M. Enthalpy–entropy and cavity decomposition of alkane hydration free energies: numerical results and implications for theories of hydrophobic solvation. *J. Phys. Chem. B* **2000**, *104*, 6271–6285.

(43) Schönbeck, C.; Westh, P.; Holm, R. Complexation thermodynamics of modified cyclodextrins: extended cavities and distorted structures. *J. Phys. Chem. B* **2014**, *118*, 10120–10129.

(44) Myers, J. K.; Pace, C. N.; Scholtz, J. M. Denaturant *m*-values and heat-capacity changes—relation to changes in accessible surface areas of protein unfolding. *Protein Sci.* **1995**, *4*, 2138–2148.

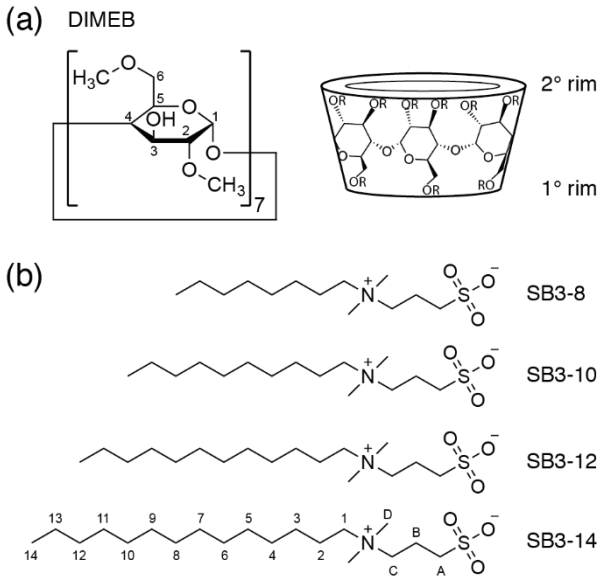

Chart 1: Chemical structures of a) heptakis(2,6-di-*O*-methyl)-β-CD (DIMEB) and b) *n*-alkyl-*N*,*N*-dimethyl-3-ammonio-1-propanesulfonate (SB3-*x*) with alkyl chains ranging in length from 8 to 14.

SB3-*x*	K_D (μM)	$\Delta G°$ (kJ mol^{-1})	$\Delta H°$ (kJ mol^{-1})	$-T\Delta S°$ (kJ mol^{-1})	ΔC_p (J mol^{-1} K^{-1})
SB3-8	1361 (1753–1009)	–16.4 (–15.7 to –17.1)	6.4 (5.3–7.7)	–22.8 (–21 to –24.8)	–375 (–454 to –309)
SB3-10	137 (157–119)	–22.1 (–21.7 to –22.4)	4.2 (4.0–4.4)	–26.3 (–25.7 to –26.8)	–486 (–507 to –466)
SB3-12	26 (30–21)	–26.4 (–25.8 to –26.7)	3.0 (2.8–3.2)	–29.4 (–28.6 to –29.9)	–581 (–600 to –563)
SB3-14	15 (19–11)	–27.6 (–27.2 to –28.3)	3.0 (2.5–3.6)	–30.6 (–29.7 to –31.9)	–664 (–676 to –566)

Table 1. Thermodynamic parameters characterizing DIMEB/SB3-*x* complexation obtained by ITC at 25°C. Measurements were performed on 5, 10, or 20 mM DIMEB and 0.5, 1, or 2 mM SB3-*x*, respectively, at 10, 18, 25, 33, 40, and 48°C. Data were fitted globally[10] to yield best-fit parameter values and 95% confidence intervals (in parentheses).

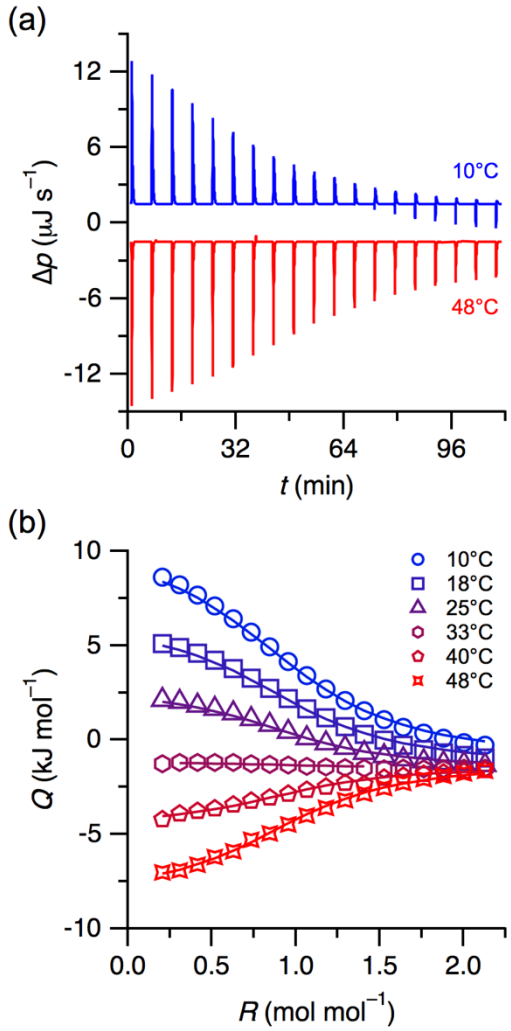

Figure 1. Formation of 1:1 DIMEB/SB3-*x* complexes. (a) Raw thermograms depicting differential heating power, Δ*p*, versus time, *t*, for 10 mM DIMEB and 1 mM SB3-10 at 10°C and 48°C. (b) Isotherms showing integrated and normalized heats of reaction, *Q*, versus DIMEB/SB3-10 molar ratio, *R*, obtained upon titrating 1 mM SB3-10 with 10 mM DIMEB at 10–48°C. Experimental data and fits assuming a 1:1 binding stoichiometry are shown as symbols and lines, respectively. Experimental uncertainties from baseline determination and peak integration for each data point are smaller than the symbols. 50 mM NaH_2PO_4/Na_2HPO_4, 50 mM NaCl, pH 7.4.

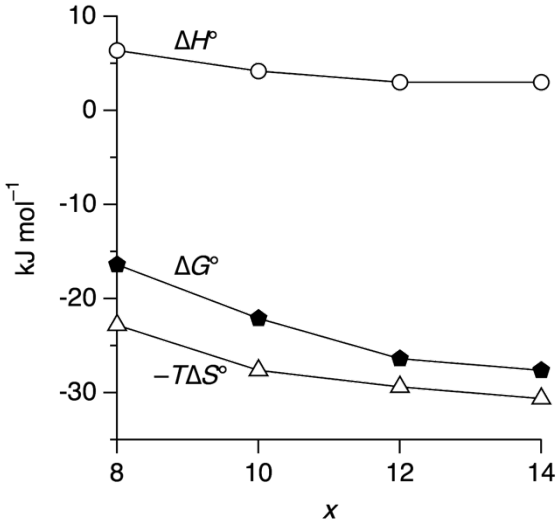

Figure 2. Thermodynamic quantities characterizing the formation of DIMEB/SB3-*x* inclusion complexes as functions of alkyl chain length, *x*, of the surfactant. 50 mM NaH_2PO_4/Na_2HPO_4, 50 mM NaCl, pH 7.4, 10–48°C.

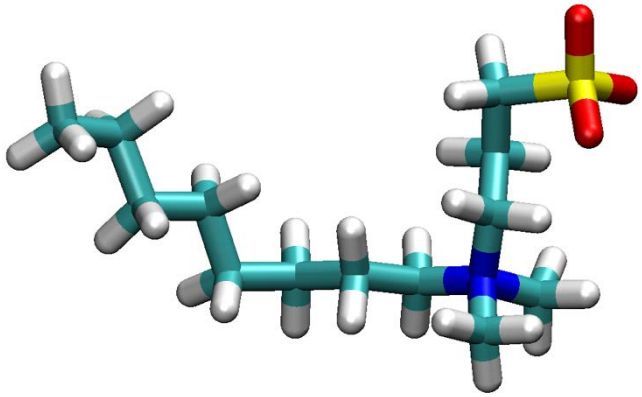

Figure 3. Typical conformation of SB3-*x* during simulation with the alkyl chain bent by ~90° about the nitrogen atom, as shown here for SB3-8.

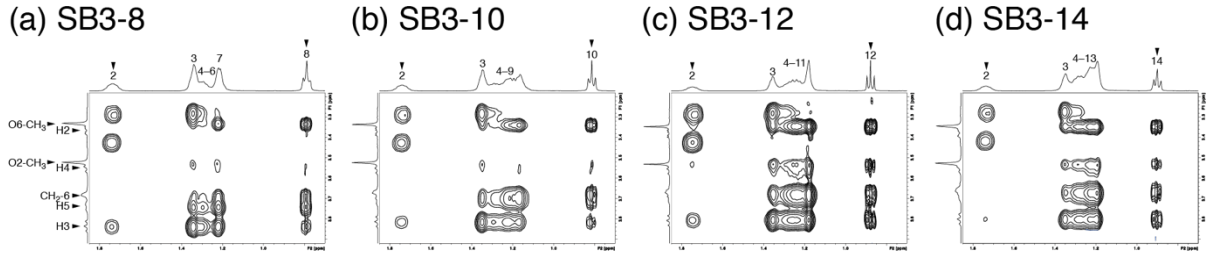

Figure 4. (a)–(d) ROESY spectra showing intermolecular cross-peaks between SB3-*x* alkyl chain protons (in particular, numbers with arrows; top projection) and DIMEB protons (labels with arrows; left projection).

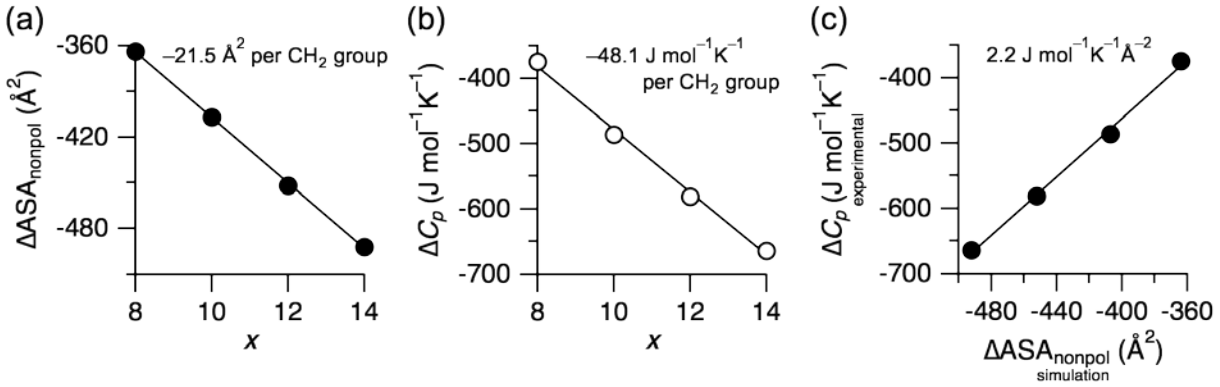

Figure 5. Relationship between ΔC_p and the amount of hydrophobic surface area buried upon binding. (a) ΔASA_{nonpol} as a function of detergent chain length, *x*, upon complexation. (b) Molar change in isobaric heat capacity, ΔC_p, as a function of alkyl chain length, *x*. (c) Correlation between ΔASA_{nonpol} and ΔC_p.

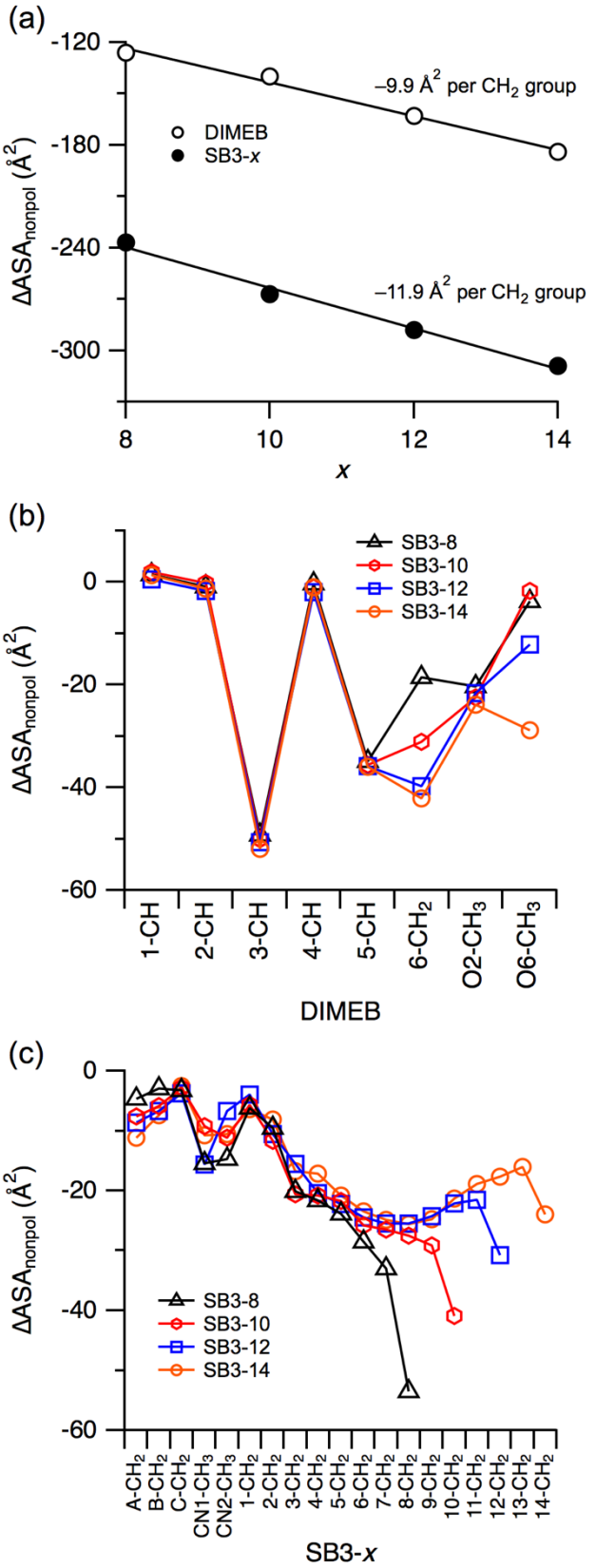

Figure 6. Analysis of individual moieties contributing to ΔASA_{nonpol}. (a) Contributions from SB3-x guest and from DIMEB host. (b) Contributions from DIMEB moieties. (c) Contributions from SB3-x moieties.

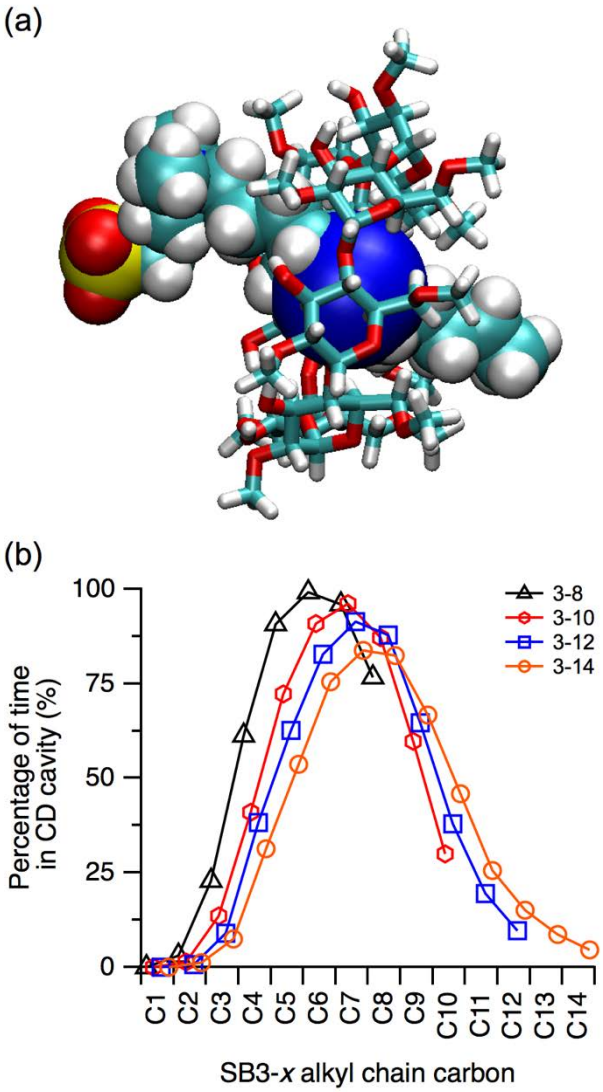

Figure 7. Analysis of SB3-*x* moieties included in the DIMEB cavity. (a) The canonical CD cavity is highlighted as a blue sphere as shown for DIMEB/SB3-12. (b) Histograms depicting the percentage of the total time spent by each carbon atom within the cavity.